

Advancing Measurement of Zero-Group-Velocity Lamb Waves Using PVDF-TrFE Transducers: First Data and Application to In-Situ Health Monitoring of Multilayer Bonded Structures

Qijian Liu^{1,+}, Yehai Li^{2,+}, Ruiqi Guan³, Jiajia Yan¹, Menglong Liu⁴, Guojie Luo⁵,
Zhongqing Su⁵, Xinlin Qing¹, Kai Wang^{1,6*}

¹ School of Aerospace Engineering, Xiamen University, Xiamen 361005, P.R. China

² Shenzhen Key Laboratory of Smart Sensing and Intelligent Systems
Shenzhen Institute of Advanced Technology, Chinese Academy of Sciences, Shenzhen
518055, P.R. China

³ College of Civil Engineering, Huaqiao University, Xiamen 361021, P.R. China

⁴ School of Mechanical Engineering and Automation, Harbin Institute of Technology,
Shenzhen 518055, P.R. China

⁵ Department of Mechanical Engineering, The Hong Kong Polytechnic University,
Kowloon, Hong Kong SAR

⁶ Innovation Laboratory for Sciences and Technologies of Energy Materials of Fujian
Province (IKKEM), Xiamen, P. R. China

Submitted to **Structural Health Monitoring- An International Journal**

(Initial submission on 21 March 2022; Revised and re-submitted on 28 July 2022)

* To whom correspondence should be addressed. Tel.: +86-15080323689;
Email: kaiwang@xmu.edu.cn (Kai WANG, *PhD*);

⁺ These authors contribute equally

1 **Abstract**

2 Driven by the rapid advancement in manufacturing technologies,
3 engineering structures with complex geometries are increasingly applied
4 in various industries, posing challenges to the applicability and adaptability
5 of existing structural health monitoring methods based on guided
6 ultrasonic waves. To fulfill the characterization of defects in complex
7 structures, a novel approach featuring a conjunction of zero-group-velocity
8 (ZGV) Lamb waves and polarized PVDF-TrFE transducers is proposed. In
9 this approach, the PVDF-TrFE solvent is deposited and in-situ polarized
10 on the structure surface to form thin and flexible coatings, with which the
11 ZGV waves can be excited efficiently and measured reliably. On this basis,
12 the defect can be characterized by investigating the defect-induced
13 alteration in ZGV wave features. In experimental validations, disbond
14 defects in multilayer bonded structures are evaluated using the ZGV waves
15 measured with fabricated PVDF-TrFE transducers. For the first time, the
16 ZGV waves are measured in a contact and in-situ manner. Compared with
17 conventional non-contact measurement of ZGV waves, the proposed
18 approach features a remarkably improved reliability, convenience for
19 narrowband excitation, immunity to measurement uncertainty and
20 capability of in-situ monitoring. The proposed approach can advance the
21 ZGV wave-based methods towards the in-situ health monitoring and
22 enable the defect evaluation in emerging complex structures.

23

24 **Keywords:** zero-group-velocity waves; PVDF-TrFE transducers; in-situ
25 health monitoring; multilayer bonded structure; disbond defects

26

27 **1. Introduction**

28 Driven by the advancements in the manufacturing technologies typified by
29 the additive manufacturing methods, structures with complex geometries
30 built as a whole are emerging recently. These structures have demonstrated
31 advantages in terms of the cost, maintenance convenience and load bearing
32 capability. Replacing conventional structures featuring assembly of simple
33 components, they are playing increasingly important roles in industries
34 including aerospace, automotive, wind energy, pressure vessel, to name a
35 few. Despite the improved properties, these emerging structures are posing
36 challenges to existing structural health monitoring technologies. Thus, it is
37 imminent to develop methods that are capable of fulfilling the structural
38 health monitoring for these complex structures.

39

40 Numerous methods exploiting the guided ultrasonic waves (GUWs) have
41 been developed and applied to detect the defects and assess the health
42 conditions of engineering structures, amongst which methods based on
43 specific wave modes have manifested applicability to structures with
44 complex geometries. For example, methods based on diffused ultrasonic
45 waves ^[1-6], featured-GUWs ^[7-9], numerical analysis-driven methods^[10-15]
46 have been intensively studied and applied. Although these methods have
47 proved their effectiveness for monitoring structures with irregular sections,
48 it is almost a consensus that the interpretation of interactions of GUWs
49 with defect in these methods is fairly challenging. This limit is further
50 stressed by the multimodal and dispersive properties of GUW, modes
51 overlapping and perplexing boundary reflections. In order to circumvent
52 this deficiency, data-driven methods have attracted numerous research
53 efforts in recent years ^[16-19]. Despite that these methods have proved their
54 applicability, they highly rely on the data used for the model training.

55 Nevertheless, the collected data are not adequate in many scenarios, and
56 more importantly, the trained model can only be applied to the structures
57 from which the data are collected. In other words, these methods are rarely
58 transferable.

59

60 Zero-group-velocity (ZGV) Lamb waves have exhibited potential for the
61 characterization of defects in complex structures. The ZGV modes are a set
62 of specific GUW modes featuring a zero energy velocity, and the energy of
63 these modes is constrained in a local region in the vicinity of the source [20,
64 21]. Upon the incidence of guided ultrasonic waves, the modes with a non-
65 zero energy velocity propagate away from the source, while the ZGV
66 modes remain in the local region, causing a local resonance. It is such a
67 feature that makes these modes only sensitive to the local material
68 properties and structural conditions, inherently immune to the perplexing
69 wave behaviors related with complex geometrical features. Leveraging the
70 features of ZGV modes, methods have been developed to enable the
71 assessment of material properties and defect identification in local regions
72 in previously challenging structures [22-26], including fairly thin structures,
73 multilayer structures, anisotropic mediums.

74

75 Nevertheless, the implementation of existing ZGV mode-based methods
76 only relies on the noncontact measurement technique [22-25], particularly the
77 noncontact laser ultrasound technique. This is attributed to the fact that the
78 mass addition and wave leakage caused by conventional bulky transducers
79 coupled to the inspected structure disturb the generation and acquisition of
80 ZGV waves significantly, as evidenced elsewhere [27]. The noncontact laser
81 ultrasound technique has demonstrated its effectiveness in investigation of
82 ZGV waves. However, devices for the laser pulse generation, beam control
83 and sensing unit are bulky and wieldy, rendering them inconvenient for the

84 in-situ measurement. To warrant the accuracy of measurement, finely
85 controlled conditions are required, considering that a number of practical
86 factors can impose salient influence on the signal acquisition, for example
87 the surface roughness, the alignment between the laser beam and surface
88 normal, the ambient conditions, the motion of inspected structure, to name
89 a few. In addition, the probing waves induced by the laser pulses are usually
90 weak due to the thermo-elastic regime requirement. These factors lead to a
91 low signal-to-noise ratio and measurement uncertainty which influences
92 the measurement precision of the ZGV wave signals in practical
93 applications. This alludes to the fact that existing measurement methods
94 for the ZGV waves cannot be applied in an in-situ and online manner.

95

96 To tackle this deficiency, the sensors permanently mounted on the
97 structures, which allow the in-situ and online excitation and sensing of
98 ZGV waves, are entailed. In order to accurately measure ZGV waves,
99 following requirements on the actuators/sensors must be satisfied: 1) the
100 actuators/sensors are sufficiently light so that their effects on the wave
101 propagation are negligible; 2) the actuators/sensors are flexible enough to
102 conform with inspected structures; 3) the actuators/sensors are capable of
103 exciting and sensing elastic waves at frequencies of ZGV modes. Recent
104 advancements in the piezoelectric film sensors and coatings based on
105 PVDF-TrFE ^[28-33], which can accommodate above requirements, have
106 opened a novel avenue for the in-situ measurement of ZGV waves. With
107 specific fabrication and processing technologies, coatings made of PVDF-
108 TrFE polymers can be polarized and demonstrate a piezoelectric effect
109 which enables its service as actuators and sensors. Flexible and light, the
110 polarized PVDF-TrFE transducers can be used to fulfill the incidence and
111 sensing of ultrasonic waves without causing excessive cost of mass
112 addition and disturbance of wave propagation. Compared with the laser

113 pulse-based approach, the polarized PVDF-TrFE transducers demonstrate
114 several remarkable advantages: 1. higher efficiency in excitation of
115 narrowband waves owing to the capability of multiple-cycle excitations;
116 2 improved sensing robustness endowed by high immunity to environment
117 noise. With the PVDF-TrFE transducers, the damage detection methods
118 base on ZGV waves can be advanced towards the in-situ health monitoring
119 of structures. However, relevant research has not been reported.

120

121 In this investigation, a method based on PVDF-TrFE transducers is
122 proposed to fulfill the in-situ measurement of ZGV waves and health
123 monitoring of complex structures. The piezoelectric PVDF-TrFE coatings
124 are fabricated on the surface of multilayer bonded structure which can act
125 as both actuators and sensors for the ZGV waves. On this basis, the defect
126 can be characterized by analyzing the obtained ZGV waves. The
127 effectiveness of the proposed approach for the defect detection is validated
128 experimentally, in which the ZGV waves in a multilayer structure are
129 obtained and the disbond defects are detected in an in-situ manner.

130 **2. Experimental Set-up**

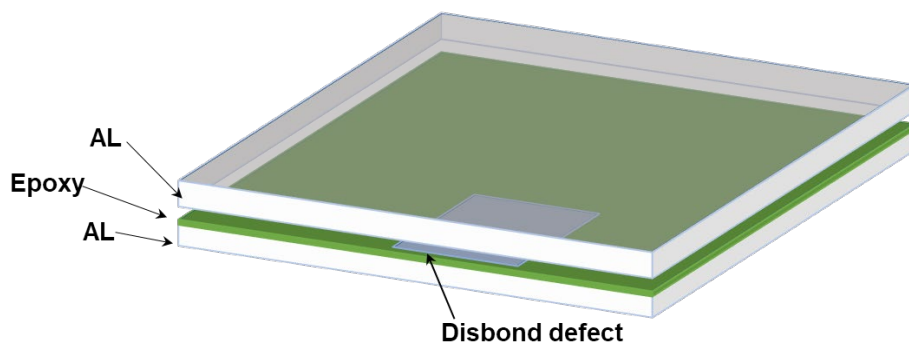
131 **2.1 Representative Sample Preparation**

132 As a representation, an adhesively bonded multilayer structure is
133 investigated in this study to validate the effectiveness of the proposed
134 method. Enabling the construction of stronger and lighter structures, the
135 adhesive bonding is a prevalently applied connection technique for
136 engineering structures in various industries including aerospace, maritime,
137 pressure vessel, etc. Considering that the multilayer bonded structure
138 consists of several layers made of at least two types of materials, the
139 interpretation of wave propagation in the structure is fairly challenging,

140 particularly in the presence of complex structural features, and therefore, it
141 is a typical engineering structure to which the real-world application of
142 conventional G UW-based SHM methods is hindered. During the
143 manufacturing and service of the multilayer bonded structures, bonding
144 degradation and disbond defect can be induced by a variety of factors, for
145 example inappropriate surface preparation, impact, cyclic loading and
146 thermal fatigue. Thus the health monitoring of multilayer bonded structures
147 is of great importance for warranting the structural integrity.

148

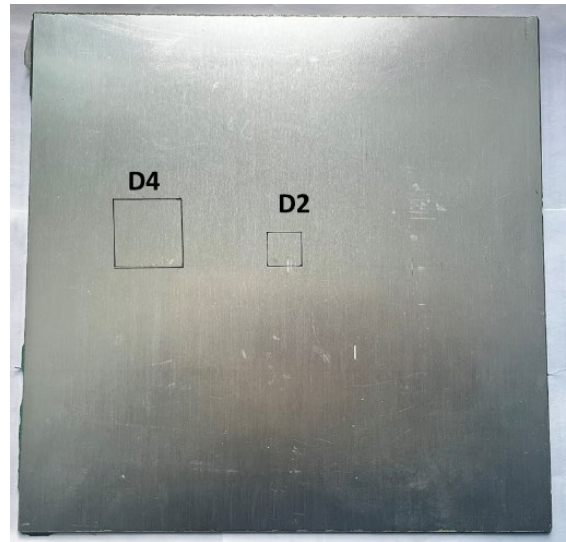
149 Without losing generality, a three layer Al-epoxy-Al bonded structure with
150 disbond defects was studied, as illustrated in Figure 1(a). In this three layer
151 bonded waveguide, two 300 mm × 300 mm aluminum plates measuring 1
152 mm in thickness were bonded using an epoxy film (Hysol PL7000) with a
153 uniform thickness of 0.2 mm. Artificial disbond defects were introduced
154 by placing Teflon inserts between one Al plate and the epoxy sheet
155 adhesive, forming unbonded surfaces. A photograph of the specimen is
156 shown in Figure 1 (b). The size of the defect is 20 mm × 20 mm and 40
157 mm × 40 mm for the disbond denoted by D2, and D4, respectively. The
158 piezoelectric coatings were fabricated on the surface of the three layer
159 bonded structure using the following method.



160

161

(a)



(b)

162

163

164 Figure 1. (a) Schematic illustration of Al-epoxy-Al bonded structure with
165 disbond defects; (b) photograph of the prepared structure with disbonds

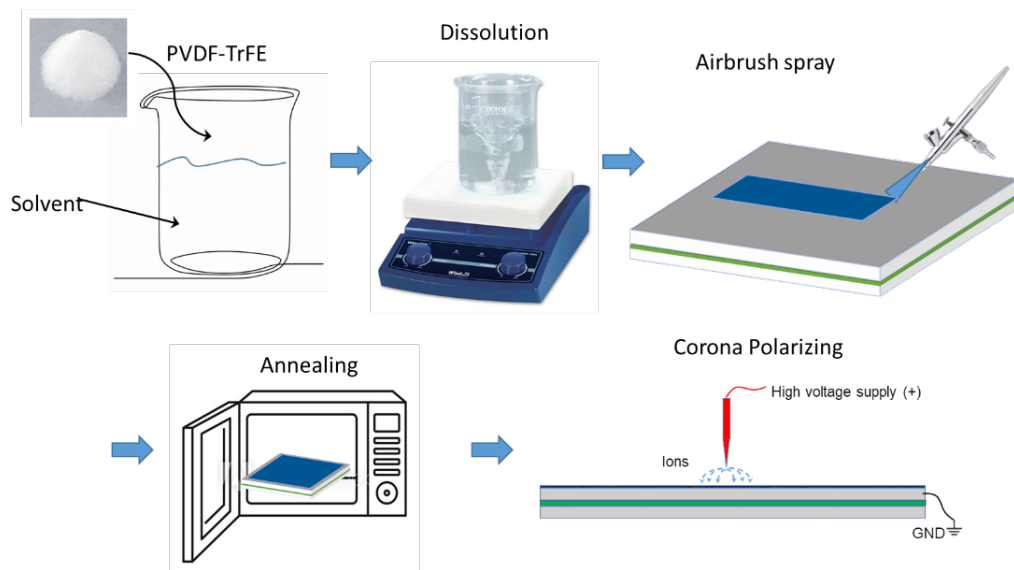
166 2.2 Fabrication of Polarized PVDF-TrFE Coatings

167 The materials PVDF-TrFE (72/28, Solvay, Belgium), acetone and DMF (N,
168 N-Dimethylformamide) with no further purification were used for the
169 fabrication of piezoelectric coatings on the surface of the multilayer
170 bonded structure.

171

172 The fabrication technique for PVDF-TrFE coatings and the effects of
173 various processing parameters on the piezoelectric properties of the film
174 was previously investigated by the authors, as reported in Li *et al*^[28], and
175 the optimized processing technique was adopted. The PVDF-TrFE
176 powders were dissolved in a mixed solvent of DMF and acetone at a
177 concentration of 5 wt%, and stirred by a magnetic stirrer for 10 hours. Then,
178 3 ml of the solution was sprayed on the surface of the structure using an
179 airbrush, after which the structure was placed in a vacuum plate to
180 evaporate the solvent and form the PVDF-TrFE coatings with thickness
181 around 80 μm . These coatings were further annealed at 135 $^{\circ}\text{C}$ for 1 hour

182 to improve the crystallinity. For electrical measurements, the silver paste
 183 was brushed on the surface of the PVDF-TrFE coatings with the aid of a
 184 shadow mask to fabricate top electrodes, and the structure served as the
 185 ground electrode owing to its conductivity. Subsequently, the PVDF-
 186 TrFE coatings were in-situ polarized by a corona discharge at 20 kV to
 187 enable the piezoelectric property. The preparation process is schematically
 188 shown in Figure 2.



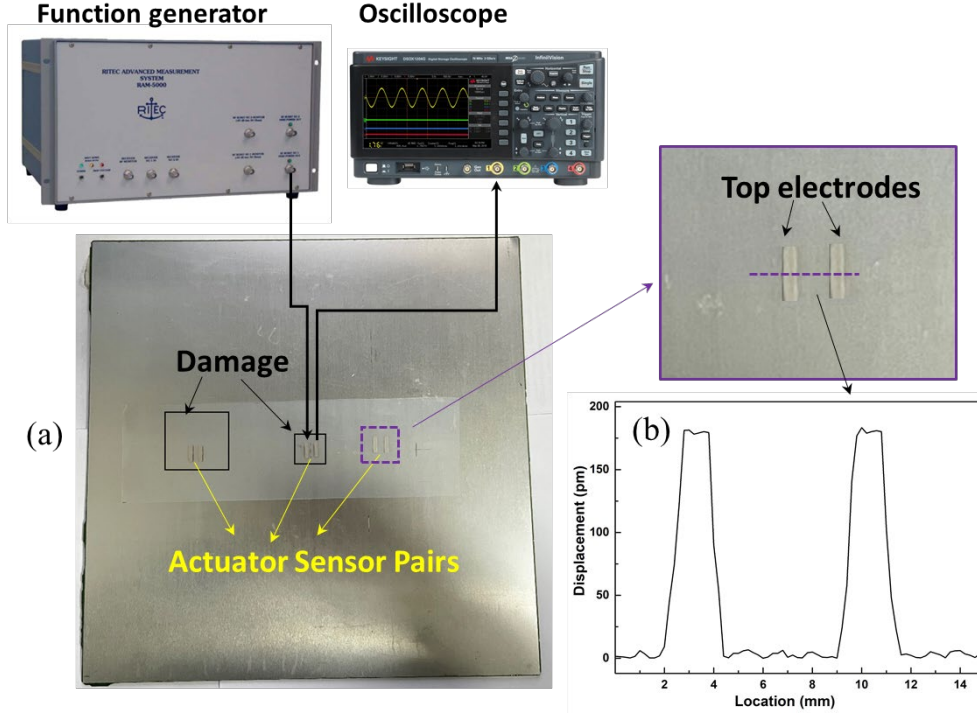
189

190 Figure 2. Schematic illustration of the in-situ fabrication of PVDF-TrFE
 191 film on the bonded structure

192

193 The effective piezoelectric coefficients of the PVDF-TrFE film were
 194 measured with a laser scanning vibrometer. A unipolar 1 kHz AC voltage
 195 of 20 V_{p-p} was applied onto the electrodes and the region with and without
 196 electrodes were scanned as shown in Figure 3. It can be observed that the
 197 effective piezoelectric coefficient d_{33} value of the fabricated coating is ~18
 198 pm/V.

199



200
 201 Figure 3. (a) Photograph of the multilayer bonded structure with
 202 piezoelectric coating on the surface acting as actuators and sensors; (b)
 203 the effective piezoelectric coefficient of piezoelectric coatings measured
 204 with laser scanning vibrometer

205 2.3 ZGV Waves in Adhesively Bonded Multilayer Structure

206 To calculate the dispersion curves of phase and group velocity of
 207 propagating modes in Al-epoxy-Al (see Figure 4), one-dimensional semi-
 208 analytical finite element method (SAFE) ^[16, 34] which is a powerful
 209 numerical method to obtain dispersion curves and mode shapes of GUW
 210 in cross section of arbitrary shape is adopted. The material parameters are
 211 listed in Table 1. In the SAFE method, the wave propagation can be
 212 depicted in an analytical form, and the displacement vector is written as

$$213 \quad u_j(x, y, z, t) = U_j(x, y) e^{i(kz - \omega t)} \quad (1)$$

214 In which k is the wavenumber, ω is the angular frequency, t is the time
 215 variable and the subscript $j=1,2,3$. The function U_j denotes the mode shape

216 in the cross-section of the waveguide, and it is incorporated in the model
 217 by a two-dimensional FE discretization.

218 With Eq. (2), the dynamic equilibrium equation of the waveguide for
 219 general anisotropic media can be written as

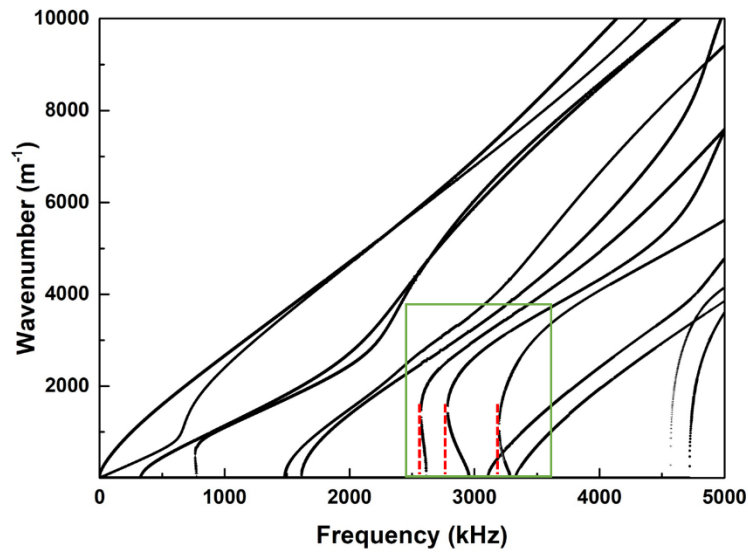
$$220 \quad C_{ijkl} \frac{\partial U_j}{\partial x_k \partial x_l} + \mathbf{I} (C_{i3jk} + C_{ikj3}) \frac{\partial (kU_j)}{\partial x_k} - kC_{i3j3} (kU_j) + \rho\omega^2 \delta_{ij} U_j = 0 \quad (2)$$

221 with summation over the indices $j=1,2,3$ and $k,l=1,2$. The coefficients
 222 C_{ijkl} denote the stiffness moduli and δ_{ij} is the Kronecker symbol.

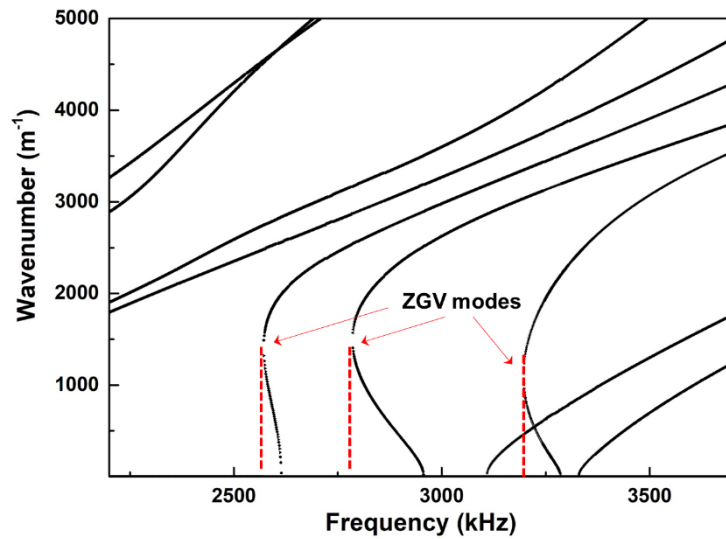
223 Equation (2) depicts an eigenvalue problem, and in the commercial FEM
 224 code^[35], the eigenvalue problems can be generally expressed in the
 225 following form

$$226 \quad \nabla \cdot (c\nabla U + \alpha U - \gamma) - \beta \nabla U - aU + \lambda d_a U - \lambda^2 e_a U = 0. \quad (3)$$

227 In the above, the expressions for all matrix coefficients can be referred to
 228 Predoi et al^[16]. By finding the eigenvalues of Eq. (3) for a given angular
 229 frequency, all the wave numbers k can be obtained, each of which
 230 represents a propagating mode at the given frequency. By finding the
 231 eigenvalue solutions over the desired range of frequencies, full dispersion
 232 curves can be obtained, as displayed in Figure 4. It is clear that three ZGV
 233 modes are present at frequencies of 2.57 MHz, 2.78 MHz and 3.2 MHz,
 234 respectively, which can be simultaneously excited by the PVDF-TrFE
 235 transducers on the surface of the structure. The corresponding wavelength
 236 of the three ZGV modes are 4.4 mm, 4.2 mm, 6.2 mm, respectively.



(a)



(b)

Figure 4. (a) The dispersion curves of Lamb waves in an intact three layer bonded structure; (b) the zoom-in view of the rectangular part in (a)

Table 1 Property parameters for the Al-Epoxy-Al structure

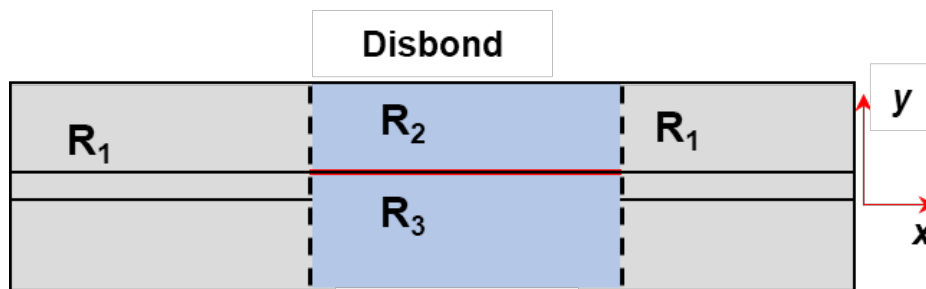
Part	Elastic modulus (GPa)	Poisson's ratio	Density (kg/m ³)
Aluminum 6061	68.9	0.33	2780
Epoxy	3.8	0.402	1104

247 The disbond defect can be modeled with unbonded surfaces between the
 248 adhesive and the adherend, which transmit no shear stress. In this scenario,
 249 the waveguide includes three regions, *i.e.* the intact bonded region denoted
 250 R_1 (Al-epoxy-Al), the upper part of disbonded region denoted R_2 (Al),
 251 and the lower part of disbonded region denoted R_3 (epoxy-Al), as denoted
 252 in Figure 5. In these three regions, guided waves propagate with different
 253 characteristics in terms of phase/group velocity dispersion curves and wave
 254 structure in the thickness direction.

255

256 Applying the same method as described above, the dispersion curves for
 257 the region R_2 and R_3 can be obtained (see Figure 6), and it can be observed
 258 that the dispersion curves in these two regions remarkably deviate from
 259 those in the intact region. Only one ZGV mode is present at the frequency
 260 of 2.64MHz for the R_3 region and 2.82MHz for the R_2 region. It can be
 261 envisioned that the energy spectrum of the dynamic responses dominated
 262 by the ZGV modes vary dramatically between the intact region and the
 263 defect region. This serves as the cornerstone for the defect detection in the
 264 adhesively bonded multilayer structures.

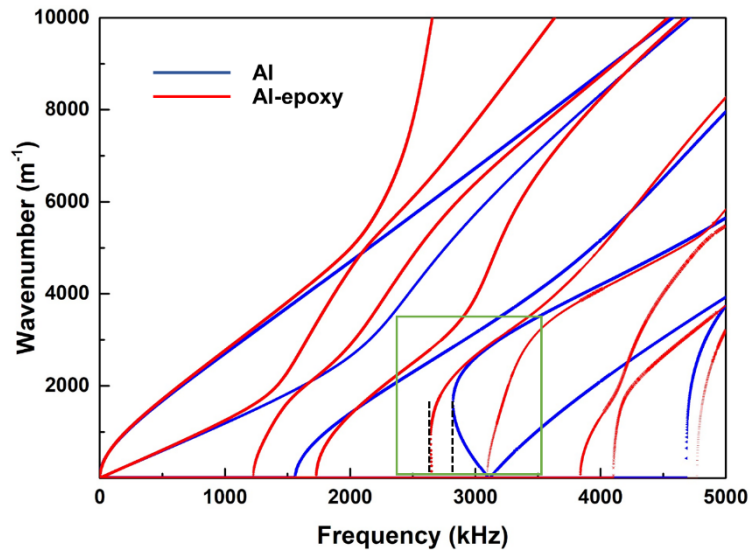
265



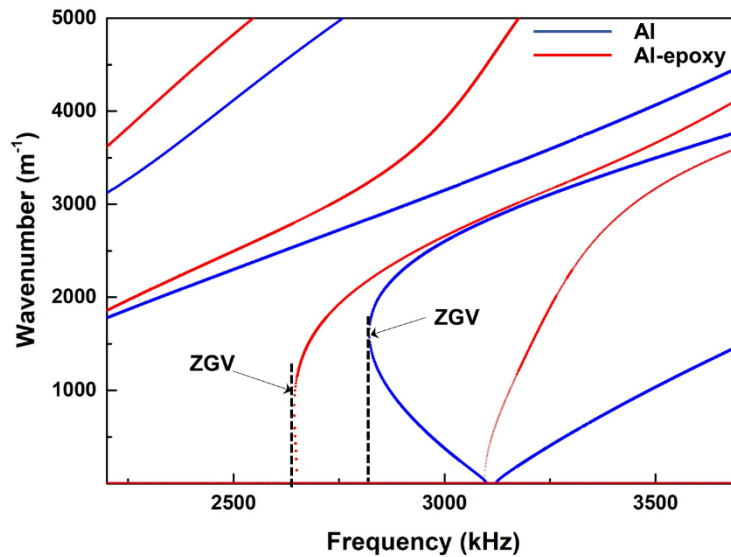
266

267 Figure 5. Schematic illustration of the three layer bonded structure
 268 bearing a disbond defect

269



(a)



(b)

Figure 6. (a) The dispersion curves of Lamb waves in intact three layer bonded structure; (b) the zoom-in view of the rectangular part in (a)

3. Results and Discussions

To excite and capture the ZGV waves, several pairs of electrodes with a size of $2\text{ mm} \times 10\text{ mm}$ were fabricated on the upper surface of PVDF-TrFE coatings in the intact and defect regions. Considering that the amplitudes of incident signals fed into the sensors ($\sim 300\text{Vpp}$) for wave excitation

281 exceed the allowable range of the oscilloscope, one of the electrodes in
282 each pair was used for the excitation and the other one for acquisition to
283 guarantee the measurement precision of ZGV waves. The distance between
284 the electrodes was 6 mm, as shown in Figure 3. The sensing pairs are
285 located near the center of each defect, and considering that the wave
286 features remain the same in the defect region, and thus the proposed
287 method is effective even when the sensing pairs are located near the
288 boundaries of defects. A ten-cycle Hanning-window modulated sinusoidal
289 tone burst with a central frequency of 3 MHz was generated using a
290 computer controlled system (Ritec[®] 5000 SNAP) and fed into the
291 electrodes of the PVDF-TrFE coatings to excite the waves in the structure.
292 The acquired waves signals were recorded via an Oscilloscope. In order to
293 increase the signal-to-noise ratio, the received signals were averaged for
294 512 times. To obtain the energy spectrum of the captured wave signals, the
295 Short Time Fourier Transform (STFT) was adopted here, which was
296 implemented using a signal processing tool Matlab(R2019b)/stft. To retain
297 sufficient details in both time and frequency domain, a temporal window
298 equivalent of three incident wave periods was selected to intercept acquired
299 signal for FFT.

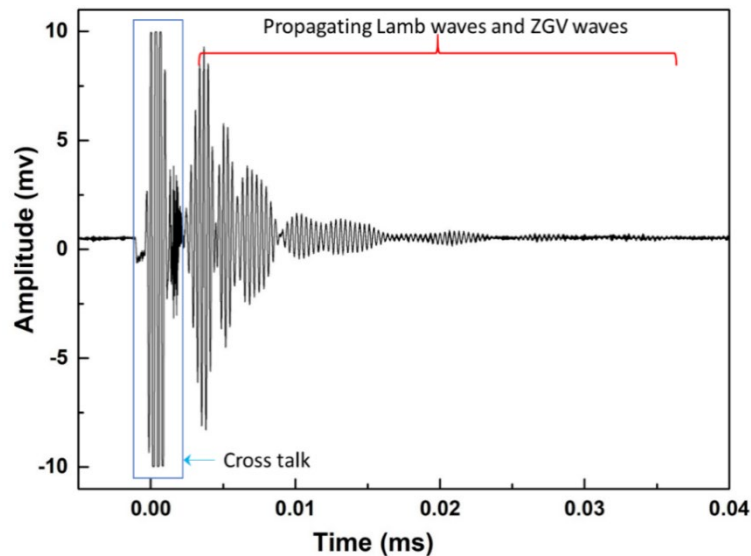
300

301 Figure 7(a) displays the wave signals obtained by the PVDF-TrFE
302 transducers in the intact region, and it can be observed that the dynamic
303 response which lasts for a long period of time before it become too weak
304 to be detected is generated. This indicates the generation of ZGV waves
305 which are constrained in the local region. The ZGV wave signals presented
306 here (Fig. 7a) are the first instance of ZGV wave measurement in a contact
307 and in-situ manner. Considering that multiple-cycle excitations can be
308 applied on the PVDF-TrFE coatings for wave incidence, local resonance
309 of ZGV waves can be generated, and thus the waves induced by the PVDF-

310 TrFE coatings can be much stronger than those by conventional non-contact
311 methods. This is beneficial for the improvement in the immunity to
312 measurement noises.

313

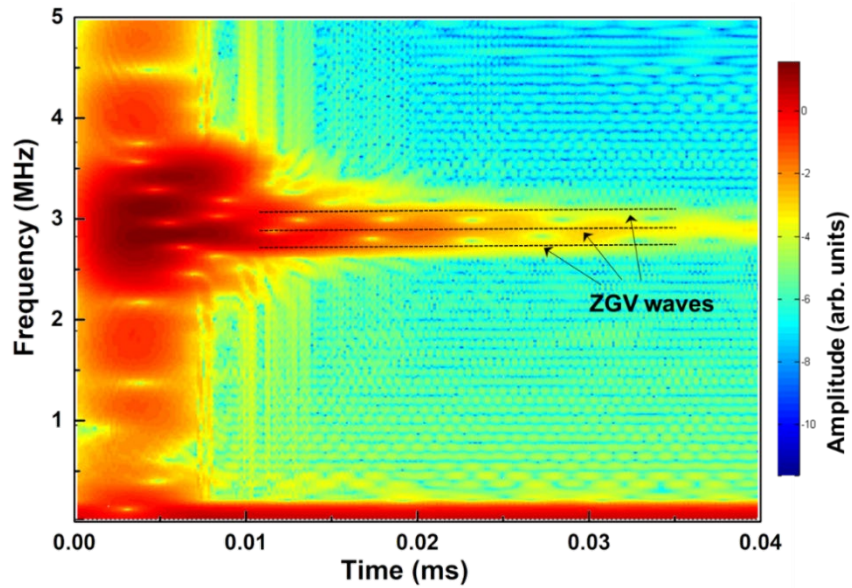
314 The corresponding spectrum obtained via the STFT are shown in Figure
315 7(b). It is clear that in the intact region, three ZGV waves are
316 synchronously excited around the frequency of 3 MHz. The frequencies of
317 three ZGV modes are 2.87MHz, 3.05MHz and 3.25 MHz, respectively,
318 which are slightly different from the theoretical predictions. This slight
319 difference might be caused by the variation in the properties of
320 adhesive/adherend layer or the bonding strength between the adhesive and
321 adherend layer. The coincidence between the theoretical predictions and
322 experimental results indicates the perfect suitability of the PVDF-TrFE
323 coatings for the measurement of the ZGV waves.



324

325

(a)



(b)

326

327

328 Figure 7. (a) The signals acquired via the sensor in the intact region; (b)

329 spectrum of the signal in (a) obtained via STFT processing

330 The spectrum of the waves acquired from D2 defect region is displayed in

331 Figure 7, and the attenuation of the three modes is clearly observed. This

332 is attributed to the fact that the wavelengths of ZGV waves are slightly

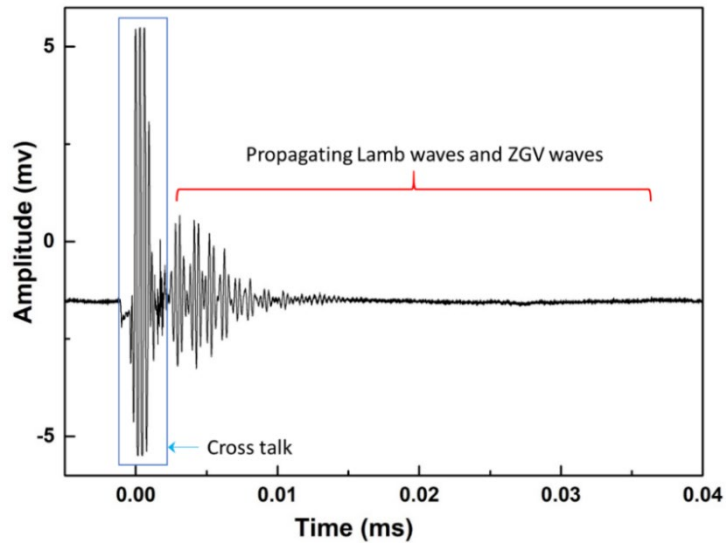
333 greater than the defect size and thus the interaction of ZGV waves with the

334 defect causes strong wave reflections and mode conversions. This leads to

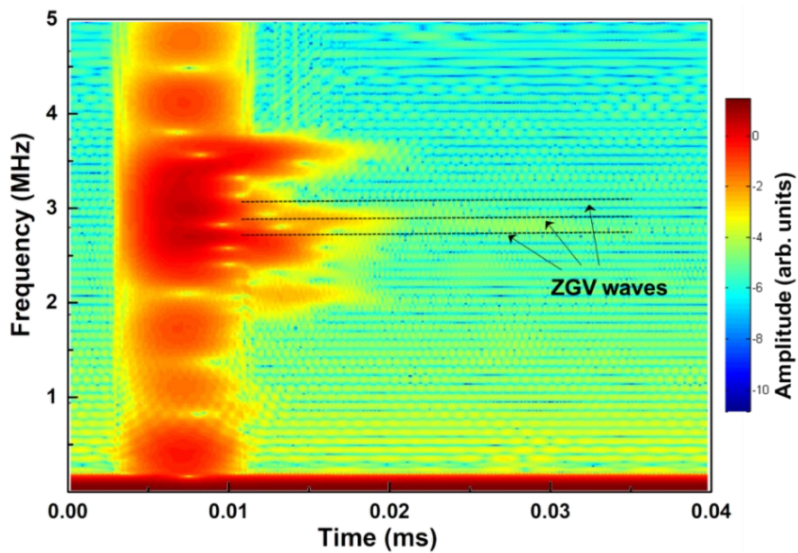
335 the remarkable energy transfer from the local resonance to the wave modes

336 which feature a non-zero energy velocity and thus propagate away from

337 the defect region, causing the attenuation of ZGV waves.



(a)



(b)

Figure 7. (a) The signals acquired via the sensor in the D2 region; (b) spectrum of the signal in (a) obtained via STFT processing

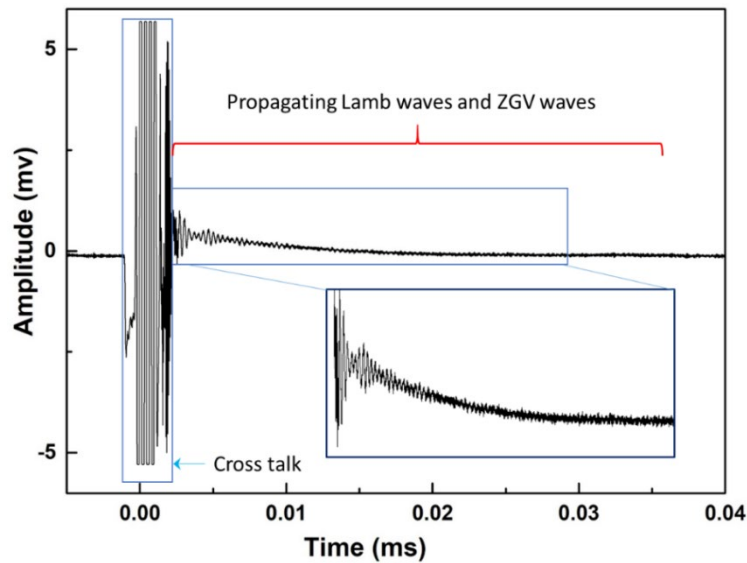
Figure 8 shows the spectrum of the waves acquired from D4 defect region, and it can be seen that only one ZGV mode with a frequency of 3 MHz dominates the response in the defect region. This is because the size of the defect is much larger than the wavelength of the ZGV waves, which guarantees the formation of the local resonance in the Al layer.

The above results indicate that the presence of defect leads to remarkable changes in the ZGV wave features. When the defect size is comparable

352 with the ZGV wavelength, significant attenuation is induced by the wave-
353 defect interaction, and when the defect size is larger than the ZGV
354 wavelength, new ZGV modes can be formed within the defect region
355 which is linked with the structural features of the defect region.

356

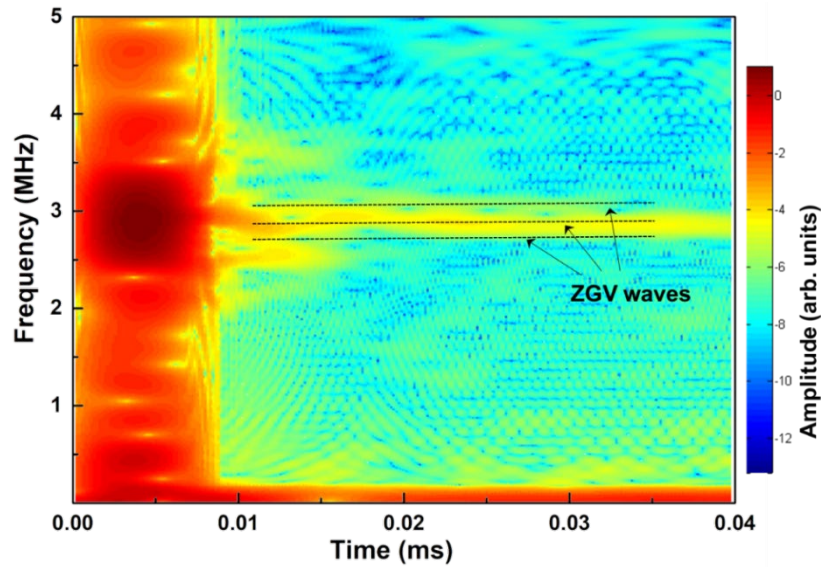
357 It is worth noting that the results from the intact and defect region
358 corroborate perfectly with the theoretical predictions, validating that the
359 lightness and flexibility of the PVDF-TrFE coatings impose negligible
360 influence on the local resonance induced by ZGV waves. This justifies the
361 effectiveness of the PVDF-TrFE transducers for the excitation and sensing
362 of ZGV waves. Therefore, the combination of the PVDF-TrFE transducers
363 and ZGV wave-based method can pave a new way for the health
364 monitoring of the structures, tackling the challenges for the existing
365 method when applied to complex structures.



366

367

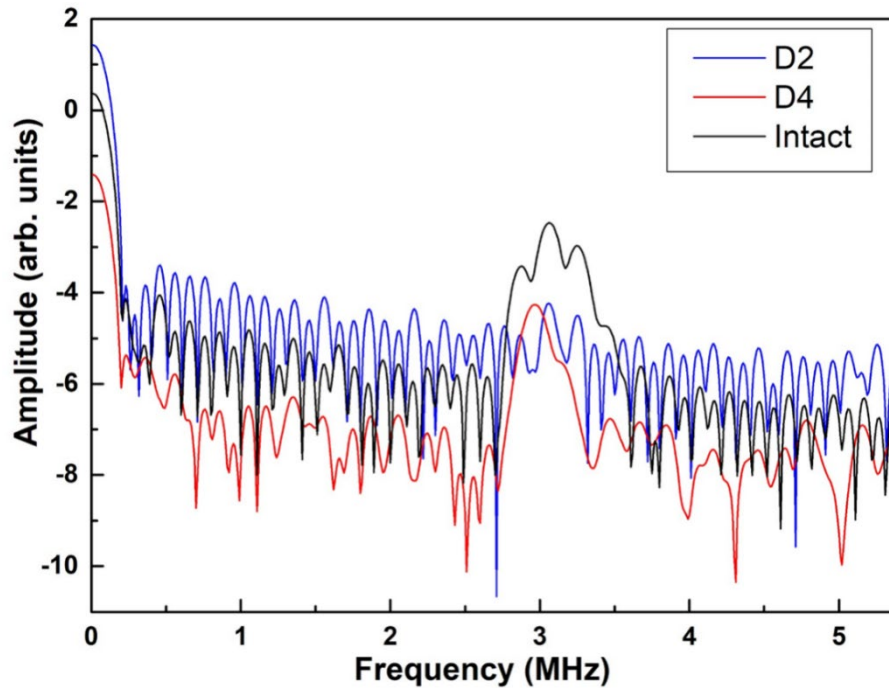
(a)



(b)

Figure 8. (a) The signals acquired via the sensor in the D4 region; (b) spectrum of the signal in (a) obtained via STFT processing

It is also noteworthy that the proposed method can enhance the robustness of the health assessment. This is attributed to the fact that the evaluation of the spectrum of ZGV waves does not entail a precise measurement of the absolute amplitude of the waves, which is a pre-requisite for numerous existing methods. As displayed in Figure 9, the amplitude of wave signals obtained from the D4 case is much lower than that in the D2 case, which is caused by the variation in the coupling conditions between the coatings and the host structure, the polarization degree and low uniformity of fabrication. Despite these uncertainties, the spectrum analysis clearly demonstrates a contrast phenomenon, a.k.a., the ZGV waves manifest outstanding dominance in the D4 case while the ZGV waves can barely be distinguished from the noise. This enhancement indicates the immunity of the proposed method to the interference related with the sensor bonding degradation and non-uniformity of fabrication, which are great concerns for conventional methods.



387
 388 Figure 9. The spectrum at 0.015ms extracted from the STFT result of
 389 signals acquired via the sensors in the intact, D2 and D4 regions
 390

391 The proposed method does not entail a repetitive scrutiny of the
 392 propagation of waves when applied to different structures with various
 393 geometrical features (*e.g.* rivet holes, stiffeners, thickness variation), which
 394 is time-consuming and challenging considering the sheer number of
 395 structures. This indicates that the proposed method can be applied in
 396 engineering practice with great convenience, featuring a potentially
 397 general applicability to the structures from various industries.

398
 399 The reliability of the proposed method will be further enhanced by
 400 improving the performance of sensors used for the wave excitation and
 401 receiving, and the sensor embedment in the adhesive layer will be
 402 investigated as well in the future work. It is clear that compared with
 403 methods based on traditional propagating guided wave modes, the
 404 detection distance of the proposed ZGV wave-based method is limited.
 405 Therefore, the proposed method is suitable for the monitoring of key sites

406 which feature stress concentration. A number of PVDF-TrFE sensors are
407 required to fulfill the monitoring of a large region.

408

409 **4. Conclusions**

410 Targeting at the in-situ health monitoring of the emerging complex
411 structures, an approach featuring a conjunction of the ZGV wave-based
412 method and flexible piezoelectric coatings is proposed. In this approach,
413 the in-situ deposited and polarized PVDF-TrFE coatings were fabricated
414 to obtain thin and flexible transducers to act as both actuators and sensors
415 for the generation and sensing of ZGV waves. On this basis, a defect
416 characterization method based on the ZGV waves was established. The
417 experimental examinations validated the efficiency and reliability of the
418 thin and flexible PVDF-TrFE coatings for the generation and sensing of
419 the ZGV waves. With the obtained ZGV waves, the disbond defects in the
420 adhesively bonded multilayer structures were characterized. Using the
421 proposed approach, the ZGV waves are measured in a contact manner for
422 the first time. Compared with conventional non-contact measurement of
423 ZGV waves, the proposed approach features a remarkably improved
424 reliability, convenience for narrowband excitation, immunity to
425 measurement uncertainty and capability of in-situ monitoring. The
426 conjunction of ZGV waves and piezoelectric polymer-driven sensors can
427 advance the ZGV wave-based methods towards the in-situ health
428 monitoring of complex structures which are emerging in diverse industries.

429

Acknowledgements

This project is supported in part by the National Natural Science Foundation of China (Grant No. 52005493), and in part by Shenzhen Stable Support Grant (Grant No. GXWD20201230155427003-20200731161831019). This project is also supported in part by Hong Kong Research Grants Council via General Research Funds (Grant Nos. 15202820, 15204419).

References

- [1] X. Chen, J. E. Michaels, S. J. Lee, and T. E. Michaels. Load-differential imaging for detection and localization of fatigue cracks using Lamb waves. *Ndt & E International* 2012; 51 142-149
- [2] A. J. Croxford, J. Cheng, and J. N. Potter, "Nonlinear phased array imaging," in *Health Monitoring of Structural and Biological Systems 2016*, 2016, p. 98052B.
- [3] J. E. Michaels and T. E. Michaels. Detection of structural damage from the local temporal coherence of diffuse ultrasonic signals. *IEEE transactions on ultrasonics, ferroelectrics, and frequency control* 2005; 52 (10):1769-1782
- [4] Y. Shen and C. E. Cesnik. Local interaction simulation approach for efficient modeling of linear and nonlinear ultrasonic guided wave active sensing of complex structures. *Journal of Nondestructive*

- [5] K. Wang, W. Cao, Z. Su, P. Wang, X. Zhang, L. Chen, *et al.* Structural health monitoring of high-speed railway tracks using diffuse ultrasonic wave-based condition contrast: theory and validation. *Smart Structures and Systems* 2020; 26 (2):227-239
- [6] K. Wang, W. Cao, L. Xu, X. Yang, Z. Su, X. Zhang, *et al.* Diffuse ultrasonic wave-based structural health monitoring for railway turnouts. *Ultrasonics* 2020; 101 106031
- [7] X. Yu, Z. Fan, M. Castaings, and C. Biateau. Feature guided wave inspection of bond line defects between a stiffener and a composite plate. *NDT & E International* 2017; 89 44-55
- [8] X. Yu, M. Ratssepp, and Z. Fan. Damage detection in quasi-isotropic composite bends using ultrasonic feature guided waves. *Composites Science and Technology* 2017; 141 120-129
- [9] Z. Zhang, Q. Li, A. Cao, W. Yeoh, M. Liu, and W. Yang. Defect identification in thick porous and wavy composites with hybrid use of ultrasound non-reciprocity and scattering. *Composites Science and Technology* 2022; 225 109514
- [10] D. Samaratunga, R. Jha, and S. Gopalakrishnan. Wavelet spectral finite element for modeling guided wave propagation and damage detection in stiffened composite panels. *Structural Health*

Monitoring 2016; 15 (3):317-334

- [11] K. Peddetti and S. Santhanam. Dispersion curves for Lamb wave propagation in prestressed plates using a semi-analytical finite element analysis. *The Journal of the Acoustical Society of America* 2018; 143 (2):829-840
- [12] A. De Luca, D. Perfetto, A. De Fenza, G. Petrone, and F. Caputo. Guided wave SHM system for damage detection in complex composite structure. *Theoretical and Applied Fracture Mechanics* 2020; 105 102408
- [13] Y. Shen and C. E. Cesnik. Hybrid local FEM/global LISA modeling of damped guided wave propagation in complex composite structures. *Smart Materials and Structures* 2016; 25 (9):095021
- [14] A. Spada, M. Capriotti, and F. Lanza di Scalea. Global–local model for three-dimensional guided wave scattering with application to rail flaw detection. *Structural Health Monitoring* 2021; 14759217211000863
- [15] K. Wang and Z. Su, "Analytical modeling of contact acoustic nonlinearity of guided waves and its application to evaluating severity of fatigue damage," in *Health Monitoring of Structural and Biological Systems 2016*, 2016, pp. 155-167.
- [16] M. V. Predoi, M. Castaings, B. Hosten, and C. Bacon. Wave propagation along transversely periodic structures. *The Journal of*

- the Acoustical Society of America* 2007; 121 (4):1935-1944
- [17] Y. Bao and H. Li. Machine learning paradigm for structural health monitoring. *Structural Health Monitoring* 2021; 20 (4):1353-1372
- [18] E. Figueiredo, G. Park, C. R. Farrar, K. Worden, and J. Figueiras. Machine learning algorithms for damage detection under operational and environmental variability. *Structural Health Monitoring* 2011; 10 (6):559-572
- [19] F.-G. Yuan, S. A. Zargar, Q. Chen, and S. Wang, "Machine learning for structural health monitoring: challenges and opportunities," in *Sensors and smart structures technologies for civil, mechanical, and aerospace systems 2020*, 2020, p. 1137903.
- [20] C. Prada, D. Clorennec, and D. Royer. Local vibration of an elastic plate and zero-group velocity Lamb modes. *The Journal of the Acoustical Society of America* 2008; 124 (1):203-212
- [21] D. Clorennec, C. Prada, and D. Royer. Local and noncontact measurements of bulk acoustic wave velocities in thin isotropic plates and shells using zero group velocity Lamb modes. *Journal of applied physics* 2007; 101 (3):034908
- [22] S. Mezil, J. Laurent, D. Royer, and C. Prada. Non contact probing of interfacial stiffnesses between two plates by zero-group velocity Lamb modes. *Applied Physics Letters* 2014; 105 (2):021605
- [23] S. Mezil, F. Bruno, S. Raetz, J. Laurent, D. Royer, and C. Prada.

- Investigation of interfacial stiffnesses of a tri-layer using Zero-Group Velocity Lamb modes. *The Journal of the Acoustical Society of America* 2015; 138 (5):3202-3209
- [24] J. Spytek, A. Ziaja-Sujdak, K. Dziedzic, L. Pieczonka, I. Pelivanov, and L. Ambrozinski. Evaluation of disbonds at various interfaces of adhesively bonded aluminum plates using all-optical excitation and detection of zero-group velocity Lamb waves. *NDT & E International* 2020; 112 102249
- [25] F. Faëse, S. Raetz, N. Chigarev, C. Mechri, J. Blondeau, B. Campagne, *et al.* Beam shaping to enhance zero group velocity Lamb mode generation in a composite plate and nondestructive testing application. *NDT & E International* 2017; 85 13-19
- [26] P. Mora, M. Chekroun, S. Raetz, and V. Tournat. Nonlinear generation of a zero group velocity mode in an elastic plate by non-collinear mixing. *Ultrasonics* 2022; 119 106589
- [27] E. Glushkov and N. Glushkova. Multiple zero-group velocity resonances in elastic layered structures. *Journal of Sound and Vibration* 2021; 500 116023
- [28] Y. Li, W. Feng, L. Meng, K. M. Tse, Z. Li, L. Huang, *et al.* Investigation on in-situ sprayed, annealed and corona poled PVDF-TrFE coatings for guided wave-based structural health monitoring: From crystallization to piezoelectricity. *Materials & Design* 2021;

199 109415

- [29] V. T. Rathod, J. K. Swamy, A. Jain, and D. R. Mahapatra. Ultrasonic Lamb wave sensitivity of P (VDF–TrFE) thin films. *ISSS Journal of Micro and Smart Systems* 2018; 7 (1):35-43
- [30] K.-W. Chen, G.-L. Chen, and C.-C. Hong. Electrodeposition of piezoelectric polymer ultrasonic transceivers for on-chip antibiotic biosensors. *Journal of the Electrochemical Society* 2016; 163 (6):B200
- [31] S. Guo, S. Chen, L. Zhang, W. H. Liew, and K. Yao. Direct-write piezoelectric ultrasonic transducers for pipe structural health monitoring. *NDT & E International* 2019; 107 102131
- [32] V.-K. Wong, M. Liu, W.-P. Goh, S. Chen, Z. Zheng Wong, F. Cui, *et al.* Structural health monitoring of fastener hole using ring-design direct-write piezoelectric ultrasonic transducer. *Structural Health Monitoring* 2022; 14759217211073950
- [33] Y. Li, K. Wang, W. Feng, H. Wu, Z. Su, and S. Guo. Insight into excitation and acquisition mechanism and mode control of Lamb waves with piezopolymer coating-based array transducers: Analytical and experimental analysis. *Mechanical Systems and Signal Processing* 2022; 178 109330
- [34] T. Hayashi, W.-J. Song, and J. L. Rose. Guided wave dispersion curves for a bar with an arbitrary cross-section, a rod and rail

example. *Ultrasonics* 2003; 41 (3):175-183

- [35] COMSOL. User's Guide and Introduction. Version 3.2 by—
COMSOLAB. <http://www.comsol.com/> Accessed on 3/5/2007 2005;